ACS APPLIED MATERIALS & INTERFACES

Research Article

www.acsami.org

Surface PEG Grafting Density Determines Magnetic Relaxation Properties of Gd-Loaded Porous Nanoparticles for MR Imaging Applications

Wuyuan Zhang,[†] Jonathan Martinelli,[†] Joop A. Peters,[†] Jacob M.A. van Hengst,[†] Hans Bouwmeester,[‡,§] Evelien Kramer,[‡] Célia S. Bonnet,[⊥] Frédéric Szeremeta,[⊥] Éva Tóth,[⊥] and Kristina Djanashvili*[,†,⊥,∥]

[†]Department of Biotechnology, Delft University of Technology, Van der Maasweg 9, 2629HZ Delft, The Netherlands

[‡]RIKILT Wageningen Research, Akkermaalsbos 2, 6708WB Wageningen, The Netherlands

[§]Division of Toxicology, Wageningen University, Stippeneng 4, 6708WE Wageningen, The Netherlands

[⊥]Centre de Biophysique Moléculaire, CNRS, Rue Charles Sadron, 45071 Orléans Cedex 2, France

[∥]Le Studium, Loire Valley Institute for Advanced Studies, 1 Rue Dupanloup, 45000 Orléans, France

S *Supporting Information*

ABSTRACT: Surface PEGylation of nanoparticles designed for biomedical applications is a common and straightforward way to stabilize the materials for in vivo administration and to increase their circulation time. This strategy becomes less trivial when MRI active porous nanomaterials are concerned as their function relies on water/proton-exchange between the pores and bulk water. Here we present a comprehensive study on the effects of PEGylation on the relaxometric properties of nanozeolite LTL (dimensions of 20 × 40 nm) ion-exchanged with paramagnetic Gd^{III} ions. We evidence that as long as the surface grafting density of the PEG chains does not exceed the "mushroom" regime (conjugation of up to 6.2 wt % of PEG), Gd-LTL retains a remarkable longitudinal relaxivity (38 s^{-1} mM^{-1} at 7 T and 25 °C) as well as the pH-dependence of the longitudinal and transverse relaxation times. At higher PEG content, the more compact PEG layer (brush regime) limits proton/water diffusion and exchange between the interior of LTL and the bulk, with detrimental consequences on relaxivity. Furthermore, PEGylation of Gd-LTL dramatically decreases the leakage of toxic Gd^{III} ions in biological media and in the presence of competing anions, which together with minimal cytotoxicity renders these materials promising probes for MRI applications.

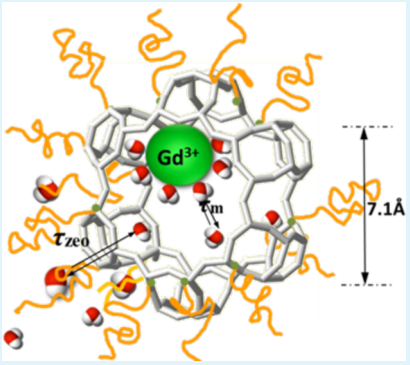

KEYWORDS: *zeolites, porous nanoparticles, water exchange, PEGylation, MRI contrast agents, relaxivity*

INTRODUCTION

A large range of nanoscale materials has been under scrutiny for their potential for tumor diagnosis and therapy over the last decades.[1−4] This interest is mainly due to (i) the ability of nanoparticles (NPs) to accumulate at the tumor sites even without targeting vectors by enhanced permeability and retention effect[5] and (ii) the possibility to combine distinct specific properties (e.g., magnetic, radioactive, or optical) resulting in multimodal probes.[6] Radiolabeled superparamagnetic iron oxide NPs,[7] magnetic quantum dots[8] or fluorescent upconversion NPs[6] are a few examples of such a multimodal approach. Additionally, surface engineering may enhance specificity of NPs and improve their performance.[9,10] In this respect, porous materials such as silica NPs and zeolites are attractive platforms to combine magnetic resonance imaging (MRI) contrast agents (CAs), optical reporters, and/or radiotracers. Mesoporous silica NPs loaded with paramagnetic Gd^{III} and doped with luminescent Eu^{III} ions have been described as dual MRI/optical imaging probes.[11] Alternatively, encapsulation of paramagnetic Gd^{III} complexes into the silica NPs results in an effective MRI CA,[12,13] while grafting of Gd^{III} and radiotracers to the surface of silica NPs allows dual application of MR and radionuclide imaging.[14]

Linde type nanozeolite (LTL) is a versatile porous material for accommodation of paramagnetic ions for MRI application.[15,16] LTL has a well-defined, negatively charged framework composed of big and small cavities that form 1D channels separated from each other and parallel to the *c*-axis of the crystals. Recently, we have demonstrated a unique strategy to achieve MRI/optical dual probe based on zeolite LTL by loading Eu^{III} and Gd^{III} ions selectively into the narrow and wide channels, respectively.[17] As the narrow channel is basically not accessible to water molecules, the luminescence quenching of Eu^{III} was effectively reduced, whereas fast exchange between the bulk water and water molecules coordinated to paramagnetic Gd^{III} ions (up to 4000 per particle) resulted in a remarkably

Received: April 28, 2017
Accepted: June 28, 2017
Published: June 28, 2017

DOI: 10.1021/acsami.7b05912
ACS Appl. Mater. Interfaces 2017, 9, 23458−23465

high relaxivity enhancement. The porous structure of LTL is superior to solid particles due to the large surface area of both internal (e.g., cavities, pores, or channels) and external surfaces. This is highly beneficial for overcoming of the intrinsic low sensitivity of MRI, since the enhancement of both the longitudinal ($1/T_1$) and the transverse ($1/T_2$) relaxation rates is linearly proportional to the number of paramagnetic ions per particle. The efficacy of a CA is assessed by its effect on water proton relaxation rates ($R_n = 1/T_n$, $n = 1$ or 2) per amount of Gd^{III} ions (s^{-1} mM^{-1}), expressed as relaxivity (r_n). A large number of parameters govern the relaxivity, of which, number of water molecules bound to Gd^{III} (q) and their residence time in the first coordination sphere (τ_m) are two dominating factors.[18] Both can be optimal in a porous structure, thus MRI CAs based on zeolites have much higher r_1 and r_2 relaxivities compared to paramagnetic complexes (e.g., Gd^{III}-DOTA) and solid NPs (e.g., Gd_2O_3).[15]

Recently, we have demonstrated that fast prototropic exchange is the origin of the exceptionally high relaxivity observed for Gd-loaded LTL (Gd-LTL) with a high pH responsiveness of both r_1 and r_2.[19] For this system (Figure 1),

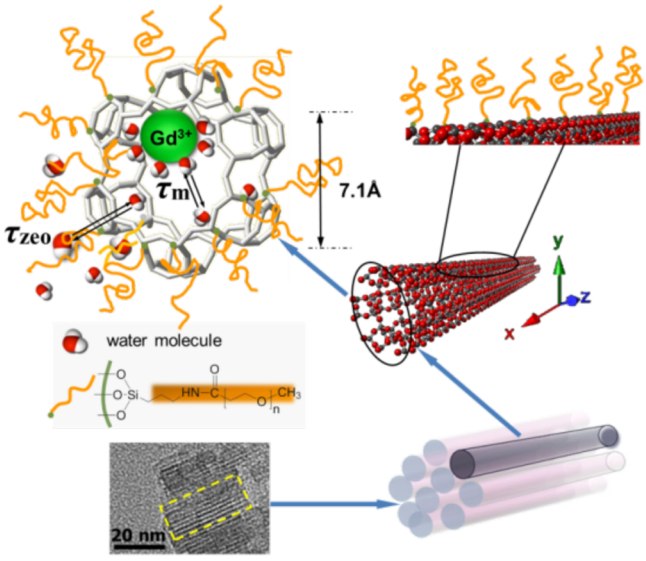

Figure 1. Schematic representation of PEGylated Gd-loaded LTL and the water exchange parameters: τ_m is the residence time of water molecules in the first coordination sphere of Gd^{III} ions and τ_{zeo} is the residence time of water molecules inside the zeolite. Only one cage unit is shown for convenience.

six water molecules in first coordination sphere of Ln^{III} in the large cages of LTL have been determined by the measurements of luminescence lifetimes of Eu^{III}.[17] The relaxivities showed a steep decrease from 38 to 8 s^{-1} mM^{-1} for r_1 and from 98 to 50 $s^{-1}mM^{-1}$ for r_2, respectively, when moving from pH 4 to 9 (7 T and 25 °C). This was explained by the exchange of water protons between the interior of the zeolite (τ_{zeo}) and bulk at pH < 6, whereas at a higher pH the exchange involves entire water molecules with a consequently much lower rate. The pH-responsive relaxivity renders Gd-LTL an interesting MRI CA for example for in vivo pH mapping of tumors, where the pH is intrinsically lower than in healthy tissues.[20] However, in vivo applications require control over biodistribution, prolonged blood circulation time,[21] and reduced toxicity[22] of the probe—all typically achieved by grafting of polyethylene glycol (PEG) to the surface of NPs. Applied to porous NPs, this may result in blockage of the channel entrance for water molecules with a negative impact on relaxivity, which has never been assessed.

In view of the high potential of porous systems as MRI CAs, we present herein a comprehensive study to assess the effects of progressive surface PEGylation of Gd-loaded LTL NPs on their relaxivity. Particularly, we have investigated the impact of PEGylation on proton exchange between bulk and encapsulated water, which represent the basis of an efficient relaxation enhancement required for MRI. The results of the present work can be readily extrapolated to other zeolite types and silica NPs designed for MRI applications.

RESULTS AND DISCUSSION

The surface of cylindrical nanoparticles of zeolite LTL with the dimensions of 20 × 40 nm loaded with Gd^{III} ions[17] was conjugated with methoxypolyethylene glycol ($mPEG_{2000}$). For the covalent attachment of PEG chains to the surface of LTL, the trimethoxysilane derivative of mPEG was prepared by conversion of $mPEG_{2000}$-OH to $mPEG_{2000}$-COOH, followed by the reaction with (3-aminopropyl)trimethoxysilane (APTMS) to form the corresponding amide (Scheme S1). The PEG-derivatives were characterized by Fourier transform infrared (FT-IR) and nuclear magnetic resonance (NMR) spectroscopies. The characteristic carbonyl stretching vibration at 1739 cm^{-1} due to the carboxylate moiety shifted down to 1657 cm^{-1} upon reaction with APTMS and consequent conversion of the COOH group into an amide (Figure S1a). Additionally, the shift of the NH_2 vibration in APTMS from 1599 to 1538 cm^{-1} in $mPEG_{2000}$-silane confirmed the formation of an amide bond. In the next step, $mPEG_{2000}$-silane was covalently attached onto Gd-LTL surface by reaction with the silanol groups present on the surface of LTL. The IR spectrum of LTL prior to PEGylation showed stretching vibrations at 3435, 1629, and bending vibrations at 1100 and 607 cm^{-1} characteristic of the Si−OH groups and $(Si/Al)O_4$ units in zeolites.[23,24] After PEGylation, a C−H stretching band at 1397 cm^{-1} and additional NH-peak at 1531 cm^{-1} confirmed the grafting (Figure S1b). The pH-dependency of the zeta-potentials also confirms PEGylation (Figure 2). Intrinsically, LTL nanocrystals possess a negative zeta potential ($\zeta = -32.2$ mV), which slightly increases after ion-exchange with Gd^{III} ($\zeta = -23.8$ mV, 5.2 wt % Gd-loading). PEGylation further reduces the overall charge ($\zeta = -16.9$ mV (6.2 wt % PEG) and −3.3 mV (9.1 wt % PEG))

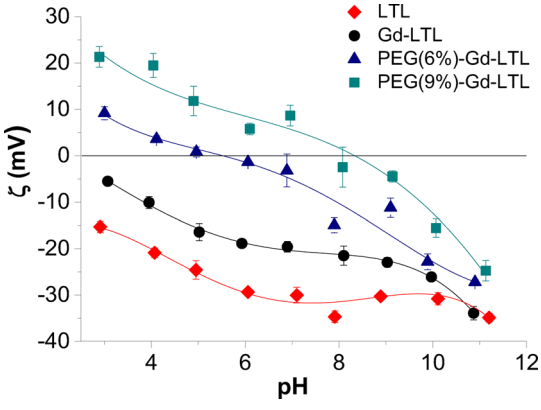

Figure 2. Zeta potential (ζ) as a function of pH: non-PEGylated LTL with 0 and 5.2 wt % Gd; PEGylated Gd-LTL (5.2 wt % Gd) with 6.2 wt % PEG and 9.1 wt % PEG. The curves are guides to the eye.

DOI: 10.1021/acsami.7b05912
ACS Appl. Mater. Interfaces 2017, 9, 23458−23465

due to the charge shielding effect.[25−27] On the one hand, native and Gd-loaded LTL samples show negative ζ in the whole pH range studied without an isoelectric point (IEP). The negative charge increasing with pH (−35 mV at pH 11) is related to the deprotonation of Si−OH groups; similar results have been observed for silanol-rich mesoporous silica NPs.[28,29] On the other hand, for PEGylated Gd-LTL, the ζ values turn from positive to negative between pH 3 and 11 with an IEP at pH 5.6 and 8.3 for 6.2 and 9.1 wt % of PEG-loading, respectively. The changeover, becoming more pronounced with increasing PEG-grafting, is in good agreement with the results by He et al., who demonstrated that mesoporous silica NPs become less negatively charged upon increase of PEG-loading.[30]

Interestingly, the ζ values of both PEGylated samples reach −27 mV at pH 11, which is only slightly above the ζ value of the non-PEGylated samples. This similarity with the non-PEGylated samples can be attributed to deprotonation of the surface Si−OH groups that remained unsubstituted by mPEG-silane as the PEG alone is not expected to contribute to the negative charge at pH 11. Consequently, the observed IEP of the PEGylated Gd-LTL samples strongly depends on degree of PEGylation, and results from an interplay between protonation of the PEG ether oxygens and deprotonation of the silanol groups.

PEG-loading was quantitatively assessed by thermogravimetric analysis (TGA) by heating freeze-dried samples from 25 up to 750 °C while monitoring the weight loss (Figure S2). The TGA profiles evidence different phases of decomposition. The first stage (<200 °C) corresponds mainly to the loss of water, physisorbed on the surface and in the pores of the zeolite. During the second stage (200−750 °C), the organic material on the surface of zeolite is decomposed and only the inorganic material remains. The TGA profiles of $mPEG_{2000}$-COOH and $mPEG_{2000}$-silane show no significant weight decrease in the first stage indicating a negligible amount of water in these samples. Between 200 and 400 °C, $mPEG_{2000}$-COOH decomposes quantitatively, whereas for $mPEG_{2000}$-silane a residue of 10−15 wt % remains. This corresponds to the amount of silane converted into silica under the measuring conditions. The changes above 600 °C observed for the LTL-samples can be attributed to the aging of the silica that gives rise to some insignificant mass decrease of the remaining material. For the entirely inorganic Gd-LTL, no weight loss was observed between 200 and 600 °C, while the loss measured for PEGylated Gd-LTL within the same temperature range indicates decomposition of the organic components. Quantification of this weight loss allows determination of the degree of PEGylation, which in this case corresponds to 8.7 wt % PEG-loading. No change in Gd-content (5.2 wt %) was induced by this PEGylation procedure, as confirmed by the paramagnetic bulk magnetic susceptibility (BMS) ^{1}H NMR shift, which is proportional to the Gd^{III}-concentration.[31]

The grafting density determines the conformation of PEG chains,[32] which in turn can influence water exchange through the pores. According to the Flory radius (R_F) theory,[22,33−35] the mushroom regime is typically expected with a low PEG-density ($D > R_F$ or $L \leq R_F$, where D is the average distance between grafting points and L is the thickness of the organic layer) when the chains fold and occupy a larger area resulting in a thin surface layer. Increasing PEG-density ($D < R_F$ or $L > 2R_F$) gradually forces the PEG chains into a brush regime with long bristles forming a thick layer on the surface.[33] Atomic force microscopy (AFM) enables determination of D, R_F, and L parameters and hence the PEG-layer thickness benefiting from an atomic-scale sensitivity/resolution and the ability to image the samples with nondestructive forces as small as 1 nN.[36] Because of the difficulties in conducting these measurements directly on the LTL NPs with small size and hydrodynamic movement in water, a commercially available silicon wafer was applied as a model. The wafer has a sufficiently flat surface and its hydrophilicity is close to that of LTL (Si/Al ratio of 3.0). Prior to PEGylation, the wafer was cleaned by oxygen plasma treatment to create a suitable water contact angle of less than 10° and increase the density of surface silanol groups.[36] After the plasma treatment, the silicon wafer was PEGylated by the same procedure as that used for LTL to yield two samples with PEG-loadings equal to LTL samples (6.2 and 9.1 wt %). The interaction forces of these model surfaces recorded in Milli-Q water in both approaching and retracting modes are displayed in Figure 3. For the flat silicon wafer without PEG chains, a typical attractive van der Waals force[37,38] was observed at a distance of 1.5 nm.

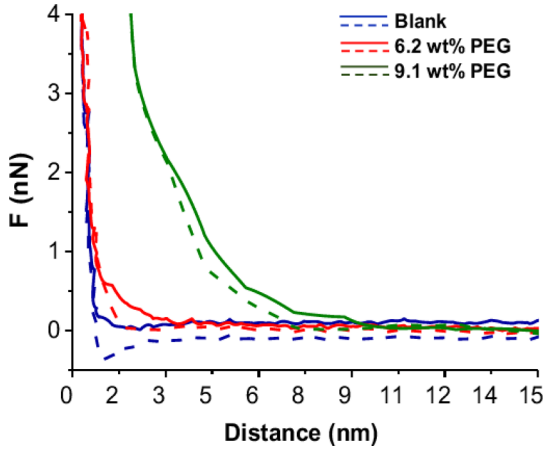

Figure 3. PEG-regimes measured as the force (F) vs the distance between the AFM tip in approaching (solid lines) and retractive (dashed lines) modes and the surface of the silicon wafer used as a model of LTL surface without PEG and with gradually increased PEG-loadings of the same wt % as it was used for conjugation with LTL.

The two PEGylated samples show different behavior. The R_F of PEG_{2000} in this work is 3.5 nm, calculated with $R_F = a \cdot n^{3/5}$ (a is the length of a monomer unit (3.5 Å for PEG), and n is the number of units (45 for PEG_{2000})). For the lower PEG-density (6.2 wt %), a PEG thickness (L) of about 2 nm corresponding to a mushroom regime ($L \leq R_F$) was directly deducted. In contrast, for the higher PEG-density (9.1 wt %), L of 9 nm was observed, which points to a brush regime ($L > R_F$). For both PEGylation regimes, the force showed an exponential decay, which is in a good agreement with the reported models[39] and the PEG thickness is consistent with the theoretical as well as the reported values for PEG_{2000}.[33,40,41] Additionally, the footprint calculated for both PEGylated materials using the surface area of a single NP (1.5×10^6 cm^2) allowed for determination of the distance between the PEG-chains, which confirmed the mushroom (D = 3.33 nm, 6.2 wt % PEG) and brush (D = 2.50 nm, 9.1 wt % PEG) regimes.

The AFM results that evidence a changeover from the mushroom to brush regime, can directly be related to the r_1 relaxivity values for aqueous suspensions of Gd-LTL with a PEG content varying from 0 to 9.1 wt % (Figure 4a). Although

DOI: 10.1021/acsami.7b05912
ACS Appl. Mater. Interfaces 2017, 9, 23458−23465

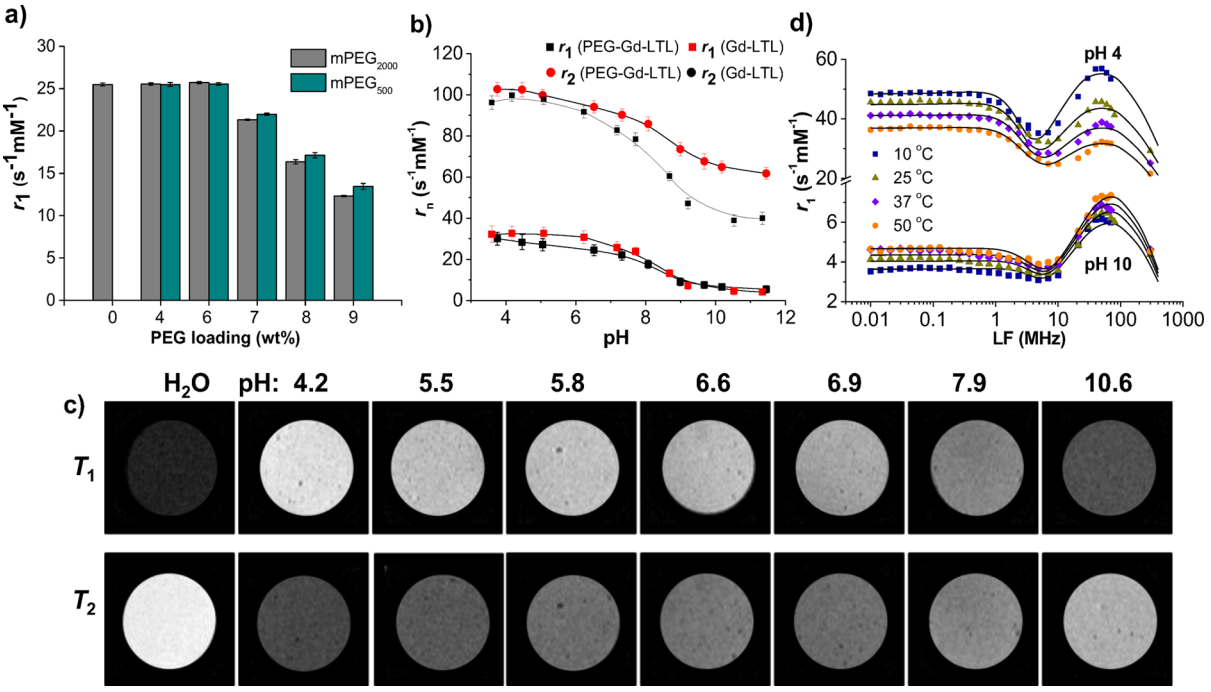

Figure 4. Relaxometric studies on aqueous suspension of Gd-loaded LTL (5.2 wt % Gd) stabilized with 0.5% xanthan solution, 300 MHz, 25 °C: (a) r_1 of Gd-LTL (pH 5.5) vs increasing loading of PEG_{2000} and PEG_{500}; (b) r_1 and r_2 of non-PEGylated and PEGylated (6.2 wt % PEG_{2000}) Gd-LTL as a function of pH (the curves are guides to the eye); (c) MR phantoms of PEGylated (6.2 wt % PEG_{2000}) Gd-LTL (0.3 mM of Gd) as a function of pH (9.4T, 25 °C), top: T_1-weighted spin−echo images, T_E = 29.9 ms; bottom: T_2-weighted images, T_R = 1 s; (d) ^{1}H NMRD profiles of PEGylated Gd-LTL (6.2 wt % PEG) at pH 4 and pH 10 and 10, 25, 37, and 50 °C. The curves were calculated with best-fit values shown in Table S2.

relaxivity remains constant (≈ 25 s^{-1} mM^{-1}) and identical to that of the non-PEGylated LTL up to 6.2 wt % PEG_{2000}, it decreases considerably at higher PEG content and drops to 12.3 s^{-1} mM^{-1} at 9.1 wt % PEG (maximum degree of PEGylation that could be reached for this zeolite). Similar behavior was observed for the Gd-LTL functionalized with shorter PEG_{500} chains, indicating no effect of the length of PEG-chains (Figure 4a). The PEG brushes compactly arranged at the surface increasingly slow down water exchange and limit water access to Gd^{III}, which explains the decline in relaxivity above 6.2 wt % PEG. Below this PEG-density, neither r_1/r_2 relaxivities nor the relaxometric pH-response are affected (Figure 4b). Our previous investigations on the relaxation mechanism revealed that above pH 7 the water structuring inside the zeolite is disrupted by ionization of the silanol groups, Gd^{III}-bound water molecules, and decreased concentration of hydronium ions.[19] This effect is less pronounced in case of the PEGylated Gd-LTL, resulting in a slightly less decrease of r_2 (Δr_2 = 22 s^{-1} mM^{-1}) compared to that of the non-PEGylated analogue (Figure 4b).

The T_1- and T_2-weighted MR images of PEG-Gd-LTL phantoms (Figure 4c) at pHs ranging from 4.2 to 10.6 are in accordance with the pH-relaxivity curves showing respective decrease and increase of the signal intensity (Table S1). Nuclear magnetic relaxation dispersion (NMRD) profiles acquired on aqueous suspensions of Gd-LTL and PEG-Gd-LTL (6.2 wt % PEG) at pH 4 and 10 to assess the rotational dynamics of the system are similar at first sight (Figure 4d and Figure S3). However, a closer inspection of their temperature dependence shows significant differences (Figure S4). At pH 4, the relaxivities of both Gd-LTL and PEG-Gd-LTL decrease with increasing temperature, which suggests that r_1 is limited by τ_M.[42] The opposite was observed for PEG-Gd-LTL at pH 10 pointing to limitation by τ_{zeo}, whereas for Gd-LTL, a transition between these two modes was found at ≈25 °C, which can most likely be ascribed to blockage of the pores by the xanthan used as dispersant for this sample (Figure S5). Fitting of the NMRD profiles at pH 4 and 10 with the 2 step model proposed previously[42] could not satisfactorily reproduce the humps around 60 MHz.

Similar phenomena were observed by Skår et al. when fitting the NMRD profiles of Gd-grafted mesoporous SBA-15 silica materials.[43] Therefore, the two-step model was completed with the Lipari−Szabo approach to describe rotational dynamics,[18] which yielded good fits. To limit the large number of parameters to be calculated in the fit, we fixed the global correlation time (τ_{gl}) that describes the motion of the zeolite nanocrystal at a value of 5×10^{-6} s, estimated via the Debye−Stokes−Einstein equation for a spherical particle with a radius of 10−40 nm

$$\tau_{gl} = \frac{4\pi a^3 \eta}{3k_B T}$$

where a is the dynamic radius of the NP, η is the shear viscosity of the surrounding fluid at temperature T, and k_B is Boltzmann's constant.

Analysis of the NMRD profiles, described in detail in the Supporting Information, includes the best-fit parameters summarized in Table S2 and the curves calculated with these parameters are given in Figure 4d and Figure S6. The data clearly indicate a dramatic increase of τ_{zeo} from pH 4 to 10, which is then responsible for the large relaxivity decrease. As shown previously,[19] this is due to a changeover in the proton exchange mechanism between the zeolite cavities and the bulk from prototropic to undissociated water exchange.

DOI: 10.1021/acsami.7b05912
ACS Appl. Mater. Interfaces 2017, 9, 23458−23465

For Gd-LTL at pH, given the possible blocking of the pores by xanthan, the NMRD profiles were fitted separately at each temperature. Nevertheless, the tendency in τ_{zeo} is consistent with the same change in the proton exchange mechanism. The τ_{loc} correlation time probably corresponds to the motion of the Gd−H vector of the Gd^{III} aqua ion within the pores. Because the model applied is rather crude and has many assumptions, the best fit parameters should be considered with caution.[44] They seem, however, to be consistent with the model proposed previously.[19] At pH 10, all τ_{loc} values obtained are unreasonably small. This might be related to a compensation in the fit for an incorrectly high hydration number. Indeed, based on the luminescence data, q was fixed at 6 for both pH values, although a lower q cannot not be excluded as the Gd-coordinated water can partially deprotonate at basic pH.

The integrity of Gd-loaded LTL in water, saline, serum, and lactate solutions was assessed after 24 h of incubation at 37 °C by calorimetric assay.[45] It revealed a significant reduction of free Gd^{III} ions release in the case of PEGylated analogues. The decreased negative surface charge obviously reduces ion-exchange with electrolytic cations present in physiological media and, as a result, the leakage even under the harshest conditions (saline) drops down to 3 wt % Gd corresponding to 1.2×10^{-8} mol L^{-1} (Figure S7). To verify this, in another experiment, LTL particles were first PEGylated, and then subjected to ion-exchange. In this way, only 0.42 wt % Gd could be loaded into LTL, instead of 5.2 wt % of Gd for the "naked" LTL under the same conditions. This indeed confirms the protecting effect of the PEG layer against leaching through ion-exchange.

Another concern is the possible blockage of the pore entrances by various molecules having affinity for the surface of porous materials. We have previously found that stabilizing aqueous suspensions of Gd-LTL with 0.5 wt % xanthan gum (a common agent for the dispersion of NPs) does perturb the relaxivities, particularly at higher temperatures.[19] In the presence of xanthan, both r_1 and r_2 of Gd-LTL are constant over time at 25 °C, whereas they are continuously decreasing at 50 °C, and after cooling back the sample to 25 °C, the relaxivities are lower than the original values. Interestingly, relaxivity remains reproducible when Gd-LTL is incubated at 50 °C for 1 h in water and the xanthan gum is added only after cooling back to 25 °C. These findings evidence that xanthan interacts with the pores of the zeolite LTL and partially blocks them at higher temperatures. When carrying out similar variable temperature experiments with a PEGylated Gd-LTL (6.2 wt % PEG) in the presence of xanthan, relaxivities remain reproducible and stable in time (Figure S5). The absence of interaction between the PEGylated zeolite LTL and xanthan is remarkable. First, it evidences that the relaxation effect of Gd-NPs is related to proton exchange between the pores and bulk water. Second, it confirms that a PEG layer, even in a mushroom configuration (with 6.2 wt % PEG), can efficiently protect the particles from interferences with different solutes without affecting relaxivity.

The results demonstrate that no changes in hydrodynamic size occur over 24 h. This allowed further in vitro assessment of the cytotoxicity by viability tests with a macrophage cell line using an ATP assay. As reported by Kihara et al., the cytotoxicity of zeolite particles is strongly dependent on morphology and size of the zeolites as well as on the type of the cell line.[46] Interestingly, these authors found a pronounced increase in toxicity for smaller particles (50 × 100 nm) compared to bigger analogues (90 × 210 nm) when incubated with HeLa cells. This is most probably due to the higher surface-to-volume ratio of the smaller particles. On the other hand, Laurent et al. reported nontoxicity of spherical LTL (18 nm) and other small zeolitic particles.[47] Another recent study demonstrates reduced toxicity of zeolite A particles (50−60 nm) after conjugation with $mPEG_{2000}$ compared to the short chain analogues.[48]

For the LTL particles with the dimensions of 20 × 40 nm used in this study no significant toxic effects were detected using macrophage cells incubated either with K-LTL (commercially available starting material) or with non-PEGylated Gd-LTL (4.3 wt % Gd) and PEGylated Gd-LTL (4.3 wt % Gd and 6.2 wt % PEG) at doses between 10 and 250 $\mu g\ mL^{-1}$ (Figure 5b). Only a slight viability decrease was

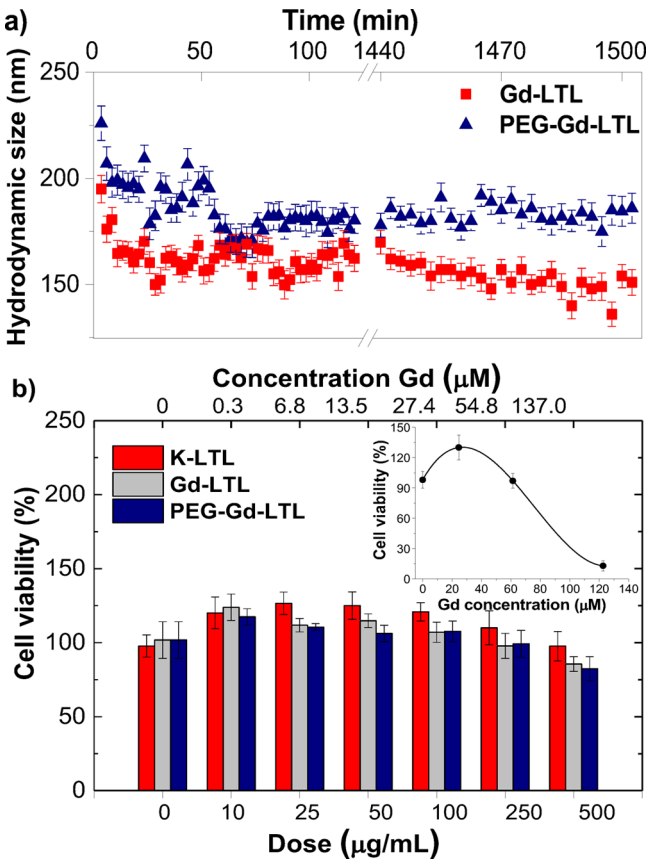

Figure 5. (a) Hydrodynamic size of non-PEGylated and PEGylated (5.2 wt % PEG) Gd-LTL samples suspended at a concentration of 750 mg mL^{-1} in DMEM (10% FCS) at 37 °C, over 24 h; (b) viability of macrophage cells incubated with K-LTL, Gd-LTL (4.3 wt % Gd), and Gd-LTL-PEG (4.3 wt % Gd and 6.2 wt % PEG) at different doses. The inset represents cell viability after incubation with increasing amount of free Gd^{III} ions.

observed at the highest dose of 500 $\mu g\ mL^{-1}$ for all the samples. The biocompatibility of PEG is already well-documented.[46] Therefore, the very similar viability results obtained in this study with both PEGylated and non-PEGylated samples suggest that the cytotoxicity of LTL itself is negligible.

CONCLUSIONS

In conclusion, we addressed the impact of progressive surface PEGylation of Gd-LTL NPs on their relaxation efficiency,

DOI: 10.1021/acsami.7b05912
ACS Appl. Mater. Interfaces 2017, 9, 23458−23465

stability and cell toxicity. A zeolite surface model allowed for direct assessment of the PEG layer thickness via AFM. It confirmed the existence of two different morphological regimes that PEG, depending on its density, can adopt on the surface of LTL particles. We evidenced that although in the mushroom PEG regime (up to 6.2 wt % PEG) the particles retain their remarkable pH-responsive relaxivity, at higher PEG density, the more compact PEG layer (brush regime) seriously limits diffusion and exchange of protons/water between the interior of LTL and the bulk. This is important guidance for surface engineering of porous NPs as potential MRI CAs in general, because their relaxation efficiency is closely related to fast exchange between bulk water and water molecules coordinated to Gd^{III} ions in the inner cavities. Even though both PEGylated and nonPEGylated Gd-LTL NPs do not induce any direct cytotoxicity up to a dose of 250 $\mu g\ mL^{-1}$, the necessity of PEGylation is clear seeing the effective reduction of interaction between the Gd-LTL NPs and surrounding molecules/ions that can (i) block the pores and reduce the relaxivity and (ii) potentially subtract/replace the encapsulated Gd^{III}. PEGylation changes the surface charge of the Gd-LTL NPs under physiological conditions and hence significantly reduces Gd^{III} leakage, which may cause a delayed in vivo toxicity.

Lanthanide-loaded LTL has already shown potential for dual T_1-T_2 MRI and optical imaging.[17,19] Here, we demonstrate the benefits of PEGylation and provide general insight into the understanding of how surface functionalization of porous nanomaterials affects fundamental properties like proton exchange as well as more applied features like MRI efficiency. We believe that this work will steer lanthanide-loaded zeolite LTL particles toward bioapplications.

EXPERIMENTAL SECTION AND METHODS

Synthesis of $mPEG_{2000}$-COOH. $mPEG_{2000}$–OH (5.00 g) was stirred in dry DMF (25 mL) at room temperature until complete dissolution occurred. NaH (461 mg, 60 wt % in oil, 11.52 mmol) was added portion-wise at 0 °C, and the resulting suspension was stirred at 0 °C for 30 min. *t*-Butyl bromoacetate (1.13 mL, 7.68 mmol) was added in once, and the mixture was stirred at room temperature under inert atmosphere for 18 h. MeOH (5 mL) was slowly poured into the reactor and the solvents were removed under reduced pressure. The residue was suspended in H_2O (40 mL) and extracted with DCM (3 × 20 mL). The organic phase was dried over anhydrous Na_2SO_4, filtered and evaporated, and the crude product was purified by column chromatography (SiO_2, DCM/MeOH 95:5, R_f = 0.2), leading to the desired compound as a yellow wax (4.03 g). This was dissolved in 1:1 TFA/DCM (20 mL), and the mixture was stirred at room temperature for 2 h. After removal of the solvents under vacuum, the product was obtained as a white solid (3.79 g) and used without further purification. ^1H NMR of $mPEG_{2000}$-COOH (400 MHz, 25 °C, D_2O), δ (ppm): 4.15 (s, 2H, CH_2COO), 3.7–3.5 (m, $C\underline{H}_2CH_2OCH_3$ + OCH_2CH_2O), 3.47 (t, $^3J_{HH}$ = 4.2 Hz, 2H, CH_2OCH_3), 3.38 (s, 3H, CH_3). ^{13}C NMR (100 MHz, 25 °C, D_2O), δ (ppm): 171.5 (CO), 71–70 (OCH_2CH_2O + $\underline{C}H_2CH_2OCH_3$ + $\underline{C}H_2OCH_3$), 69.8 (CH_2COO), 59.0 (CH_3). IR (KBr disks), cm^{-1}: 3435, 2877, 2537, 1787, 1669, 1454, 1347, 1298, 1167, 950, 848, 811, 781, 704.

Synthesis of $mPEG_{2000}$-Silane. $mPEG_{2000}$-COOH (1.0 g, 0.5 mmol) was mixed with APTMS (174 μL, 1.0 mmol) in DMF (10 mL) in the presence of HBTU (190 mg, 0.5 mmol), HOBt (68 mg, 0.5 mmol) and DIPEA (174 μL, 1 mmol) at room temperature overnight. After removal of the solvent under reduced pressure, the product was purified by dialysis (MWCO 1 kDa) followed by precipitation in Et_2O, leading to a white solid (875 mg). ^1H NMR (400 MHz, 25 °C, D_2O), δ (ppm): 0.59 ($CH_2C\underline{H}_2Si$), 1.56 ($CH_2C\underline{H}_2CH_2Si$), 2.63 ($NC\underline{H}_2CH_2CH_2$), 3.35 ($SiOCH_3$), 3.1–4.5 (mPEG-signals), 8.11 (NH).

Procedures for PEGylation of Gd^{III}-Loaded Zeolite LTL. Gd-loaded zeolite LTL (50 mg) was dispersed in a 3:2 mixture of EtOH and water (25 mL), sonicated and vigorously stirred, followed by the addition of 0.5 mL of NH_4OH (25%). To obtain different PEG-loading levels, different amounts of a 460 g L^{-1} $mPEG_{2000}$-silane stock solution in water were added to the particle suspension (e.g., 25 μL for 6.2% PEG-loading). The mixture was gently stirred for 24 h and then centrifuged, washed with water (3×) and freeze-dried.

Stability Assessment. The assessment of leaching of Gd^{III} ions was performed on zeolite dispersions (1.5 mg mL^{-1}) in water, physiological saline (0.9 w/v %), serum (20 v/v %), and lactate (2.5 mM), respectively. After being incubated in a shaker at 37 °C for 24 h, the supernatant was collected and analyzed by the xylenol orange complexation method using UV–vis spectroscopy, as previously reported.[45]

Cytotoxicity Test. Fifteen milligrams of lyophilized native zeolite K-LTL, Gd-LTL, and PEG-Gd-LTL NPs were suspended in 1 mL of filter-sterile water containing 0.05% bovine serum albumin (BSA). These stock suspensions were sonicated for 10 min at 20 °C in a Branson 5510 water bath sonicator (Emerson, USA) at 100% output (4W specific ultrasound energy, 240 J/m^3). The suspensions were transferred into glass vials and the total volume was adjusted to 3 mL with 0.05% BSA (the final concentration of the stock suspensions was 5000 $\mu g\ mL^{-1}$). Mouse macrophage cells RAW 264.7 (ATCC TIB-71) were obtained from the American Type Culture Collection, (ATCC, Manassas, VA). Cells were used at passages 8 and 10. RAW 264.7 cells were cultured in Dulbecco's Modified Eagle's Medium (DMEM; 4.5 g L^{-1} glucose, w/o L-glutamine, w/o phenol red, Lonza, Verviers, Belgium) supplemented with glutamax (Gibco). Also, penicillin-streptomycin (PEST; 1% v/v; Sigma, St. Louis, MO), and heat-inactivated fetal bovine serum (FBS; 10% v/v; Gibco) were added to the medium. Cells were incubated at 37 °C in a humidified environment (95% relative humidity) and 5% carbon dioxide with a Thermo Scientific HERAcell 240. Cells were passed at 80% confluency by subcultivation at a 1:6 ratio twice a week until use. All media and solutions were prewarmed to 37 °C before use.

The viability was assessed using the ATPlite assay (PerkinElmer). 100 μL suspensions with a concentration of 2 × 10^4 cells/mL were seeded in 96 wells white plates with clear bottom (Costar) (6250 cells/well). After 48 h, these cells reached a confluency of 30%. To assess the possible cytotoxic effect of the NPs on RAW264.7 cells, a dilution range of 10, 25, 50, 100, 250, and 500 μg/mL nanoparticles (corresponding to 2.87, 7.17, 14.3, 28.7, 71.7, and 143.4 μM Gd) was added to the cells for 24 h. Next, 50 μL of mammalian cell lysis solutions were added to 100 μL of cell suspension, and incubated for 5 min in an orbital shaker at 700 rpm. Subsequently, 50 μL of substrate solution were added, followed by shaking for another 5 min at 700 rpm, and a final incubation in the dark for 10 min. Chemo-luminescence was measured at 590 nm. A control of NPs without cells, showed no interference of the NPs with the ATPlite assay.

Relaxometric Studies and ^1H NMRD Profiles. The samples were prepared by dispersing 2.5 mg of Gd-LTL or PEGylated Gd-LTL nanoparticles in 1.0 mL of Milli-Q water using a sonication bath and stabilized by adding 1.0 g of 1% xanthan gum solution. The pH of the samples was adjusted by addition of either 0.1 M HCl or 0.1 M NaOH. The pH dependence of longitudinal (r_1) and transversal (r_2) relaxivities was investigated on a Varian Inova 300 NMR spectrometer at 25 °C. After careful shimming, the line widths and peak positions were determined by fitting Lorenzian functions to the ^1H NMR spectra. Longitudinal relaxation times were measured with the inversion recovery method,[49] whereas transverse relaxation times were measured with the Carr–Purcell–Meiboom–Gill (CPMG) pulse sequence in which the length of the spin echo train was varied[50] with an echo time of 0.5 ms applied.^1H NMRD profiles were acquired on a fast field-cycling Stelar SmartTracer relaxometer with magnetic field varying from 0.00024 to 0.25 T (0.001 to 10 MHz ^1H Larmor frequencies). Additional data points in the range of 20–70 MHz were collected on a Bruker WP80 NMR electromagnet, as well as a separate point at 300 MHz on a Varian Inova 300 NMR spectrometer.

DOI: 10.1021/acsami.7b05912
ACS Appl. Mater. Interfaces 2017, 9, 23458–23465

MR Imaging. MRI experiments were conducted on a BioSpec 94/21, 9.4 T horizontal magnet (Bruker BioSpin, Wissembourg, France) equipped with BG060 gradient system (950 mT m^{-1} maximal strength and 60 mm inner diameter) and Paravision 5.1 software (Bruker BioSpin). T_1- and T_2-weighted MR images were acquired with spin–echo sequence (RARE sequence with one echo to get a small echo time (T_E) and to make the effective-T_E equal to T_E) at 25 °C. T_1-weighted images were acquired with 29.9 ms T_E and varying T_R (repetition time) and from 37 to 1500 ms, 137 × 137 mm^2 resolution with a matrix 256 × 256 in 16 min acquisition. T_2-weighted images were acquired with varying TE from 19.9 to 79.60 ms, T_R of 1000 ms, and 137 × 137 mm^2 resolution with a matrix 256 × 256 in 19 min. All images have 1.0 mm slice thickness.

■ ASSOCIATED CONTENT

Supporting Information

The Supporting Information is available free of charge on the ACS Publications website at DOI: 10.1021/acsami.7b05912.

Synthetic schemes, IR spectra, TGA profiles, time-/temperature-dependent relaxivity measurements and fittings (PDF)

■ AUTHOR INFORMATION

Corresponding Author

*E-mail: k.djanashvili@tudelft.nl.

ORCID

Joop A. Peters: 0000-0001-8503-1452

Kristina Djanashvili: 0000-0003-1511-015X

Author Contributions

The manuscript was written through contributions of all authors. All authors have given approval to the final version of the manuscript.

Notes

The authors declare no competing financial interest.

■ ACKNOWLEDGMENTS

This research was performed in the framework of the EU COST Action TD1004, "Theranostics Imaging and Therapy: an Action to Develop Novel Nanosized Systems for Imaging-Guided Drug Delivery", and was supported by China Scholarship Council (W.Z.), The Netherlands Organization for Scientific Research NWO (K.D. Veni grant-722.012.009), and the Dutch Ministry of Economic Affairs (E.K. and H.B.). The authors thank Prof. Mauro Botta (University of Eastern Piedmont, Alessandria, Italy) for the access to the relaxometry equipment.

■ REFERENCES

(1) Chen, G.; Qiu, H.; Prasad, P. N.; Chen, X. Upconversion Nanoparticles: Design, Nanochemistry, and Applications in Theranostics. *Chem. Rev.* **2014**, *114*, 5161–5214.

(2) Gallo, J.; Long, N. J.; Aboagye, E. O. Magnetic Nanoparticles as Contrast Agents in the Diagnosis and Treatment of Cancer. *Chem. Soc. Rev.* **2013**, *42*, 7816–7833.

(3) Howes, P. D.; Chandrawati, R.; Stevens, M. M. Bionanotechnology. Colloidal Nanoparticles as Advanced Biological Sensors. *Science* **2014**, *346*, 1247390.

(4) Kim, T. J.; Chae, K. S.; Chang, Y.; Lee, G. H. Gadolinium Oxide Nanoparticles as Potential Multimodal Imaging and Therapeutic Agents. *Curr. Top. Med. Chem.* **2013**, *13*, 422–433.

(5) Cheng, Z.; Al Zaki, A.; Hui, J. Z.; Muzykantov, V. R.; Tsourkas, A. Multifunctional Nanoparticles: Cost Versus Benefit of Adding Targeting and Imaging Capabilities. *Science* **2012**, *338*, 903–910.

(6) Cheng, L.; Yang, K.; Li, Y.; Chen, J.; Wang, C.; Shao, M.; Lee, S.-T.; Liu, Z. Facile Preparation of Multifunctional Upconversion Nanoprobes for Multimodal Imaging and Dual-Targeted Photothermal Therapy. *Angew. Chem., Int. Ed.* **2011**, *50*, 7385–7390.

(7) Torres Martin de Rosales, M.; Tavare, R.; Paul, R. L.; Jauregui-Osoro, M.; Protti, A.; Glaria, A.; Varma, G.; Szanda, I.; Blower, P. J. Synthesis of ^{64}Cu(II)-bis(dithiocarbamatebisphosphonate) and its Conjugation with Superparamagnetic Iron Oxide Nanoparticles: in Vivo Evaluation as Dual-Modality PET-MRI Agent. *Angew. Chem., Int. Ed.* **2011**, *50*, 5509–5513.

(8) Jing, L.; Ding, K.; Kershaw, S. V.; Kempson, I. M.; Rogach, A. L.; Gao, M. Magnetically Engineered Semiconductor Quantum Dots as Multimodal Imaging Probes. *Adv. Mater.* **2014**, *26*, 6367–6386.

(9) Erathodiyil, N.; Ying, J. Y. Functionalization of Inorganic Nanoparticles for Bioimaging Applications. *Acc. Chem. Res.* **2011**, *44*, 925–935.

(10) Groult, H.; Ruiz-Cabello, J.; Pellico, J.; Lechuga-Vieco, A. V.; Bhavesh, R.; Zamai, M.; Almarza, E.; Martin-Padura, I.; Cantelar, E.; Martinez-Alcazar, M. P.; Herranz, F. Parallel Multifunctionalization of Nanoparticles: A One-Step Modular Approach for in Vivo Imaging. *Bioconjugate Chem.* **2015**, *26*, 153–160.

(11) Tse, N. M. K.; Kennedy, D. F.; Kirby, N.; Moffat, B. A.; Muir, B. W.; Caruso, R. A.; Drummond, C. J. Mesoporous Europium-Gadolinosilicate Nanoparticles as Bimodal Medical Imaging Agents and a Potential Theranostic Platform. *Adv. Healthcare Mater.* **2013**, *2*, 836–845.

(12) Taylor, K. M. L.; Kim, J. S.; Rieter, W. J.; An, H.; Lin, W.; Lin, W. Mesoporous Silica Nanospheres as Highly Efficient MRI Contrast Agents. *J. Am. Chem. Soc.* **2008**, *130*, 2154–2155.

(13) Wartenberg, N.; Fries, P.; Raccurt, O.; Guillermo, A.; Imbert, D.; Mazzanti, M. A Gadolinium Complex Confined in Silica Nanoparticles as a Highly Efficient T_1/T_2 MRI Contrast Agent. *Chem. - Eur. J.* **2013**, *19*, 6980–6983.

(14) Laprise-Pelletier, M.; Bouchoucha, M.; Lagueux, J.; Chevallier, P.; Lecomte, R.; Gossuin, Y.; Kleitz, F.; Fortin, M.-A. Metal Chelate Grafting at the Surface of Mesoporous Silica Nanoparticles (MSNs): Physico-Chemical and Biomedical Imaging Assessment. *J. Mater. Chem. B* **2015**, *3*, 748–758.

(15) Peters, J. A.; Djanashvili, K. Lanthanide Loaded Zeolites, Clays, and Mesoporous Silica Materials as MRI Probes. *Eur. J. Inorg. Chem.* **2012**, *2012*, 1961–1974.

(16) Tsotsalas, M.; Busby, M.; Gianolio, E.; Aime, S.; De Cola, L. Functionalized Nanocontainers as Dual Magnetic and Optical Probes for Molecular Imaging Applications. *Chem. Mater.* **2008**, *20*, 5888–5893.

(17) Mayer, F.; Zhang, W.; Brichart, T.; Tillement, O.; Bonnet, C. S.; Toth, E.; Peters, J. A.; Djanashvili, K. Nanozeolite-LTL with Gd^{III} Deposited in the Large and EuIII in the Small Cavities as a Magnetic Resonance Optical Imaging Probe. *Chem. - Eur. J.* **2014**, *20*, 3358–3364.

(18) Toth, E.; Helm, L.; Merbach, A. In *Relaxivity of Gadolinium(III) Complexes: Theory and Mechanism*; John Wiley & Sons: New York, 2013; Chapter 2, pp 25–81.

(19) Zhang, W.; Peters, J. A.; Mayer, F.; Helm, L.; Djanashvili, K. Prototropic Exchange Governs T_1 and T_2 Relaxivities of a Potential MRI Contrast Agent Nanozeolite Gd-LTL with a High pH Responsiveness. *J. Phys. Chem. C* **2015**, *119*, 5080–5089.

(20) Tannock, I. F.; Rotin, D. Acid pH in Tumors and its Potential for Therapeutic Exploitation. *Cancer Res.* **1989**, *49*, 4373–4384.

(21) Pernia Leal, M.; Rivera-Fernandez, S.; Franco, J. M.; Pozo, D.; de la Fuente, J. M.; Garcia-Martin, M. L. Long-circulating PEGylated Manganese Ferrite Nanoparticles for MRI-Based Molecular Imaging. *Nanoscale* **2015**, *7*, 2050–2059.

(22) Jokerst, J. V.; Lobovkina, T.; Zare, R. N.; Gambhir, S. S. Nanoparticle PEGylation for Imaging and Therapy. *Nanomedicine* **2011**, *6*, 715–728.

(23) Das, S. K.; Mahanta, S. P.; Bania, K. K. Oxidative Coupling of 2-Naphthol by Zeolite-Y Supported Homo and Heterometallic Trinuclear Acetate Clusters. *RSC Adv.* **2014**, *4*, 51496–51509.

(24) Zecchina, A.; Otero Arean, C. Diatomic Molecular Probes for Mid-IR Studies of Zeolites. *Chem. Soc. Rev.* **1996**, *25*, 187−197.
(25) Mannisto, M.; Vanderkerken, S.; Toncheva, V.; Elomaa, M.; Ruponen, M.; Schacht, E.; Urtti, A. Structure-Activity Relationships of Poly(L-Lysines): Effects of Pegylation and Molecular Shape on Physicochemical and Biological Properties in Gene Delivery. *J. Controlled Release* **2002**, *83*, 169−182.
(26) Ogris, M.; Brunner, S.; Schuller, S.; Kircheis, R.; Wagner, E. PEGylated DNA/Transferrin-PEI Complexes: Reduced Interaction with Blood Components, Extended Circulation in Blood and Potential for Systemic Gene Delivery. *Gene Ther.* **1999**, *6*, 595−605.
(27) Petersen, H.; Fechner, P. M.; Martin, A. L.; Kunath, K.; Stolnik, S.; Roberts, C. J.; Fischer, D.; Davies, M. C.; Kissel, T. Polyethylenimine-Graft-Poly(ethylene glycol) Copolymers: Influence of Copolymer Block Structure on DNA Complexation and Biological Activities as Gene Delivery System. *Bioconjugate Chem.* **2002**, *13*, 845−854.
(28) Colilla, M.; Izquierdo-Barba, I.; Sanchez-Salcedo, S.; Fierro, J. L. G.; Hueso, J. L.; Vallet-Regi, M. Synthesis and Characterization of Zwitterionic SBA-15 Nanostructured Materials. *Chem. Mater.* **2010**, *22*, 6459−6466.
(29) Musso, G. E.; Bottinelli, E.; Celi, L.; Magnacca, G.; Berlier, G. Influence of Surface Functionalization on the Hydrophilic Character of Mesoporous Silica Nanoparticles. *Phys. Chem. Chem. Phys.* **2015**, *17*, 13882−13894.
(30) He, Q.; Zhang, J.; Shi, J.; Zhu, Z.; Zhang, L.; Bu, W.; Guo, L.; Chen, Y. The Effect of PEGylation of Mesoporous Silica Nanoparticles on Nonspecific Binding of Serum Proteins and Cellular Responses. *Biomaterials* **2010**, *31*, 1085−1092.
(31) Corsi, D. M.; Platas-Iglesias, C.; Van Bekkum, H.; Peters, J. A. Determination of Paramagnetic Lanthanide(III) Concentrations from Bulk Magnetic Susceptibility Shifts in NMR Spectra. *Magn. Reson. Chem.* **2001**, *39*, 723−726.
(32) Perry, J. L.; Reuter, K. G.; Kai, M. P.; Herlihy, K. P.; Jones, S. W.; Luft, J. C.; Napier, M.; Bear, J. E.; DeSimone, J. M. PEGylated PRINT Nanoparticles: The Impact of PEG Density on Protein Binding, Macrophage Association, Biodistribution, and Pharmacokinetics. *Nano Lett.* **2012**, *12*, 5304−5310.
(33) Damodaran, V. B.; Fee, C. J.; Ruckh, T.; Popat, K. C. Conformational Studies of Covalently Grafted Poly(ethylene glycol) on Modified Solid Matrices Using X-ray Photoelectron Spectroscopy. *Langmuir* **2010**, *26*, 7299−7306.
(34) De Gennes, P. G. Polymers at an Interface; a Simplified view. *Adv. Colloid Interface Sci.* **1987**, *27*, 189−209.
(35) Marsh, D.; Bartucci, R.; Sportelli, L. Lipid Membranes with Grafted Polymers: Physicochemical Aspects. *Biochim. Biophys. Acta, Biomembr.* **2003**, *1615*, 33−59.
(36) Ducker, W. A.; Senden, T. J.; Pashley, R. M. Direct Measurement of Colloidal Forces Using an Atomic Force Microscope. *Nature* **1991**, *353*, 239−241.
(37) Deryagin, B.; Landau, L. Theory of the Stability of Strongly Charged Lyophobic Sols and of the Adhesion of Strongly Charged Particles in Solutions of Electrolytes. *Acta Physicochim.* **1941**, *14*, 633−662.
(38) Verwey, E. J. W.; Overbeek, J. T. G. Theory of the Stability of Lyophobic Colloids. *Colloid Polym. Sci.* **1955**, *141*, 44−45.
(39) Al-Hashmi, A. R.; Luckham, P. F. Using Atomic Force Microscopy to Probe the Adsorption Kinetics of Poly(ethylene oxide) on Glass Surfaces from Aqueous Solutions. *Colloids Surf., A* **2012**, *393*, 66−72.
(40) Heuberger, M.; Drobek, T.; Spencer, N. D. Interaction Forces and Morphology of a Protein-resistant poly(ethylene glycol) Layer. *Biophys. J.* **2005**, *88*, 495−504.
(41) Xu, Z.; Marchant, R. E. Adsorption of Plasma Proteins on Polyethylene Oxide-Modified Lipid Bilayers Studied by Total Internal Reflection Fluorescence. *Biomaterials* **2000**, *21*, 1075−1083.
(42) Platas-Iglesias, C.; VanderElst, I.; Zhou, W. Z.; Muller, R. N.; Geraldes, G. C.; Maschmeyer, T.; Peters, J. A. Zeolite GdNaY Nanoparticles with Very High Relaxivity for Application as Contrast Agents in Magnetic Resonance Imaging. *Chem. - Eur. J.* **2002**, *8*, 5121−5131.
(43) Skar, H.; Liang, Y.; Erichsen, E. S.; Anwander, R.; Seland, J. G. Relaxometric Properties of Gadolinium-Grafted Mesoporous SBA-15 Silica Materials with Varying Pore Size. *Microporous Mesoporous Mater.* **2013**, *175*, 125−133.
(44) Peters, J. A. The Reliability of Parameters Obtained by Fitting of ^{1}H NMRD Profiles and ^{17}O NMR Data of Potential Gd^{3+}-Based MRI Contrast Agents. *Contrast Media Mol. Imaging* **2016**, *11*, 160−168.
(45) Barge, A.; Cravotto, G.; Gianolio, E.; Fedeli, F. How to Determine Free Gd and Free Ligand in Solution of Gd Chelates. A Technical Note. *Contrast Media Mol. Imaging* **2006**, *1*, 184−188.
(46) Kihara, T.; Zhang, Y.; Hu, Y.; Mao, Q.; Tang, Y.; Miyake, J. Effect of Composition, Morphology and Size of Nanozeolite on its in Vitro Cytotoxicity. *J. Biosci. Bioeng.* **2011**, *111*, 725−730.
(47) Laurent, S.; Ng, E. P.; Thirifays, C.; Lakiss, L.; Goupil, G. M.; Mintova, S.; Burtea, C.; Oveisi, E.; Hebert, C.; de Vries, M.; Motazacker, M. M.; Rezaee, F.; Mahmoudi, M. Corona Protein Composition and Cytotoxicity Evaluation of Ultra-Small Zeolites Synthesized from Template free Precursor Suspensions. *Toxicol. Res.* **2013**, *2*, 270−279.
(48) Męczyńska-Wielgosz, S.; Piotrowska, A.; Majkowska-Pilip, A.; Bilewicz, A.; Kruszewski, M. Effect of Surface Functionalization on the Cellular Uptake and Toxicity of Nanozeolite A. *Nanoscale Res. Lett.* **2016**, *11*, 123.
(49) Vold, R. L.; Waugh, J. S.; Klein, M. P.; Phelps, D. E. Measurement of Spin Relaxation in Complex Systems. *J. Chem. Phys.* **1968**, *48*, 3831−3832.
(50) Meiboom, S.; Gill, D. Modified Spin-Echo Method for Measuring Nuclear Relaxation Times. *Rev. Sci. Instrum.* **1958**, *29*, 688−691.

DOI: 10.1021/acsami.7b05912
ACS Appl. Mater. Interfaces 2017, 9, 23458−23465